Influence of *Adansonia digitata* Stem Extract Immersion Time on Properties of Biosynthesised Silver Nanoparticles

Sabastine Ezike [1]
https://orcid.org/0000-0003-3962-1624
sabastine.ezike@mau.edu.ng

Mustafa S. Adamu [1]

Emmanuel Ike [1]
https://orcid.org/0000-0003-4388-7150

Mufutau A. Salawu [2]
https://orcid.org/0000-0001-7523-3173

Pascal Timtere [1]
https://orcid.org/0009-0002-3698-5334

Raphael Mmaduka Obodo [3]
https://orcid.org/0000-0001-7418-8526

Abstract

The emergence of the multidisciplinary field of nanoscience with potential applications in medicine, cosmetics, renewable energy, agriculture and environmental remediation has led scientists to search for safer methods of synthesising nanoparticles. We based this study on the synthesis of silver nanoparticles (AgNPs) for varying immersion times of 30, 60, 90, 120 and 150 min, while employing *Adansonia digitata* as a reducing and capping agent and labelled A, B, C, D and E, respectively. The X-ray diffraction (XRD) pattern of the synthesised AgNPs for all samples have three peaks positioned at $2\theta = 37.94°$, 44.07° and 64.37° corresponding to (111), (200) and (220) planes, respectively. The samples have a preferred orientation at $2\theta = 37.94°$ corresponding to (111) plane irrespective of the duration of immersion of *Adansonia digitata* root extracts. The preferred intense peak shows a polycrystalline phase composition of the green synthesised AgNPs, demonstrating the creation of face-centred cubic crystalline of AgNPs. The intrinsic stress, σ_s, dislocation density, δ, specific surface area, S, crystallite size (D), surface area (S) to volume (V) ratio, lattice parameter, *a* and atomic packing factor were calculated from XRD data and presented. The particle sizes obtained

1 Department of Physics, Modibbo Adama University, Nigeria.
2 Department of Physics, University of Ilorin, Nigeria.
3 Department of Physics, University of Nigeria.

UNISA university of south africa PRESS
Nano-Horizons
Volume 3 | 2024 | 12 pages

Nano-Horizons
https://doi.org/10.25159/3005-2602/15935
ISSN 3005-2602 (Online)

from the SEM analysis are 69.88, 18.69, 15.45, 19.64 and 20.08 nm for samples A, B, C, D and E, respectively. The optical energy band gaps are 2.37 eV, 2.42 eV, 2.59 eV, 2.52 eV and 2.34 eV for samples A, B, C, D and E respectively. The synthesised AgNPs can be used in energy storage and conversions owing to their properties.

Keywords: *Adansonia digitata* root; baobab plant root; green synthesis; immersion time; reducing agent; silver nanoparticles

Introduction

Nanotechnology and nanomaterial have become a tool in the hand of researchers worldwide to further science and technology. Nanoparticles are crucial to the development of robust and environmentally friendly human technology in the future, particularly the field of green chemistry [1], [2]. One of the most significant areas for researchers is the synthesis of metal nanoparticles and the expansion of their various applications in the industrial, pharmaceutical and biomedical engineering sectors [3], [4] and specific applications can be traced in wastewater remediation [5], [6], cosmetics [7] and corrosion inhibition [8]. The broad range of applications that nanoparticles hold in the fields of biology, chemistry, physics and medicine make their production and characterisation extremely interesting [9]. Silver nanoparticles (AgNPs) are gaining increased attention owing to their beneficial properties, which include high surface-to-volume ratios, catalytic abilities, and antimicrobial effects on silver [10]. Unfortunately, the majority of nanoparticle manufacturing methods are costly and have the potential to negatively affect biological systems and the environment. In contrast, green synthesis provides a safer and more environmentally friendly method of synthesising nanoparticles [11].

Several attempts have been made in the past five years to develop more economical and ecologically acceptable processes for producing nanoparticles [12]. Because they may produce a large variety of secondary metabolites with a significant reduction power, plants present a highly suitable mechanism for the synthesis of nanoparticles. Plants provide a more environmentally friendly option for the biosynthesis of AgNPs than algae [13], diatoms [14], [15], yeast [16], fungi [17] and bacteria [18] because they are less susceptible to the harmful effects of metals. Because they provide capping layers to nanoparticles, medicinal herbs are useful since they can regulate the size and form of nanoparticles [19]. Rich resources are available from plant secondary products for use as food additives, nutraceuticals, and even medications. Among the many types of naturally occurring secondary metabolites that are antioxidants are plant polyphenols [20]. The reducing properties of these antioxidant metabolites may be related to the increased ability of plant extracts to produce nanoparticles with superior properties [21].

Nevertheless, the properties and uses of metal nanoparticles depend critically on the inorganic metal ions present, leading to a sharp rise in the size of the surface area of a particle. The result may lead to the emergence of novel optical properties, improved

thermal and electrical conductivities, a lowered melting point and other qualities [22]. Many plant extracts, such as geranium (*Pelargonium graveolens*) [23], lemongrass (*Cymbopogon flexuosus*) [24], cinnamon (*Cinnamomum camphora*) [25], neem (*Azadirachta indica*) [26], bitter leaf (*Vernonia amygdalina*), [27], aloe vera (*Aloe vera*) [28], tamarind (*Tamarindus indica*) [29], and the fruit extract of *Emblica officinalis* [30], have proven effective in producing nanoparticles by fast and efficient extracellular production.

Baobab (*Adansonia digitata*) is a plant that is readily available in Yola, Adamawa State, Nigeria. The leaves, pod fibres (from fruits), stem bark and roots of *Adansonia digitata* trees are beneficial to humans [31]. *Adansonia digitata* leaf has a wide range of uses as reducing agent in biological processes, corrosion inhibitors [32] and materials for optoelectronic devices [33].

These characteristics motivated us to investigate the synthesis of *Adansonia digitata* root extract, which provides new opportunities for a range of applications in diverse disciplines. The effective antioxidant activity and capacity for phenolic and flavonoid biosynthesis of this species [34] could be important contributors to the conversion of Ag^{+} into AgNPs. AgNPs were previously reported to have been biologically synthesised utilising *Adansonia digitata* leaf, *Adansonia digitata* fruit, *Adansonia digitata* stem (bark) and *Adansonia digitata* seed. To our knowledge, no study has attempted to synthesise AgNPs utilising *Adansonia digitata* root as the biological substrate. Consequently, the current effort, which is a novel study, used *Adansonia digitata* root extract as reducing agent to synthesise AgNPs in order to develop biologically stable AgNPs for future applications. The effect of immersion time of the *Adansonia digitata* root powder in distilled water on the properties of NPs was studied. We therefore present comprehensive results on AgNPs synthesised using the *Adansonia digitata* root extract and a variety of characterisation techniques (UV-Vis, FTIR, XRD and FESEM).

Materials and Methods

Materials Used and Preparation of *Adansonia Digitata* Root Extracts

Silver nitrate ($AgNO_3$), ethanol, distilled water and *Adansonia digitata* root were obtained. Fresh roots of *Adansonia digitata* plant (Fig. 1(a)) were collected from Sangere FUTY, which is situated between 9°20’49”N and 12°29’45”E in Girei Local Government of Adamawa State, Nigeria. As seen in Fig. 1(b), the root was cut into small pieces after being cleaned with tap water. After being cleaned, the roots were rinsed with distilled water and allowed to air dry for 14 days. Following drying, the root was ground into a powder using an electronic grinder.

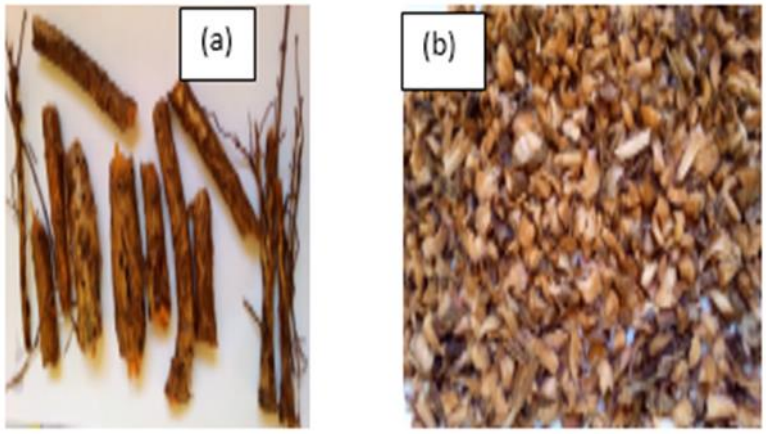

Fig. 2. (a) *Adansonia digitata* roots and (b) pieces of *Adansonia digitata* root.

A total of 5 g of the *Adansonia digitata* root powder was suspended in 50 ml of distilled water in a 250 ml conical flask. The mixture was allowed to rest for 30 min, 60 min, 90 min 120 min, and 150 min, for immersion time optimisation. Then it was filtered, labelled A, B, C, D and E, respectively, and stored in the refrigerator for further use. The extracts are shown in Fig. 2.

Fig. 1. *Adansonia digitata* root extracts.

Synthesis of AgNPs

$AgNO_3$ precursor and extract from the roots of *Adansonia digitata* were used to create the AgNPs. Using a magnetic stirrer, 5 g of a produced plant extract was dissolved in 50 ml of $AgNO_3$ (0.1 M) while being continuously stirred at room temperature. Within an hour, the pale yellow colour of the solution gradually changed to a dark brown colour. It was regarded as an obvious indicator of AgNP growth. Following the completion of the reaction, the solution was given time to settle before the supernatant was carefully removed. The mixture was centrifuged for 40 min at 5 000 rpm, and the supernatant was removed after three thorough washes. Washing was done to get rid of the by-product. Ultimately, it was dried in an oven and dehydrated with ethanol. $AgNO_3$ is completely converted into AgNPs after drying, and the NPs are then kept for characterisations. The entire process of AgNPs synthesis is summarised in Fig. 3.

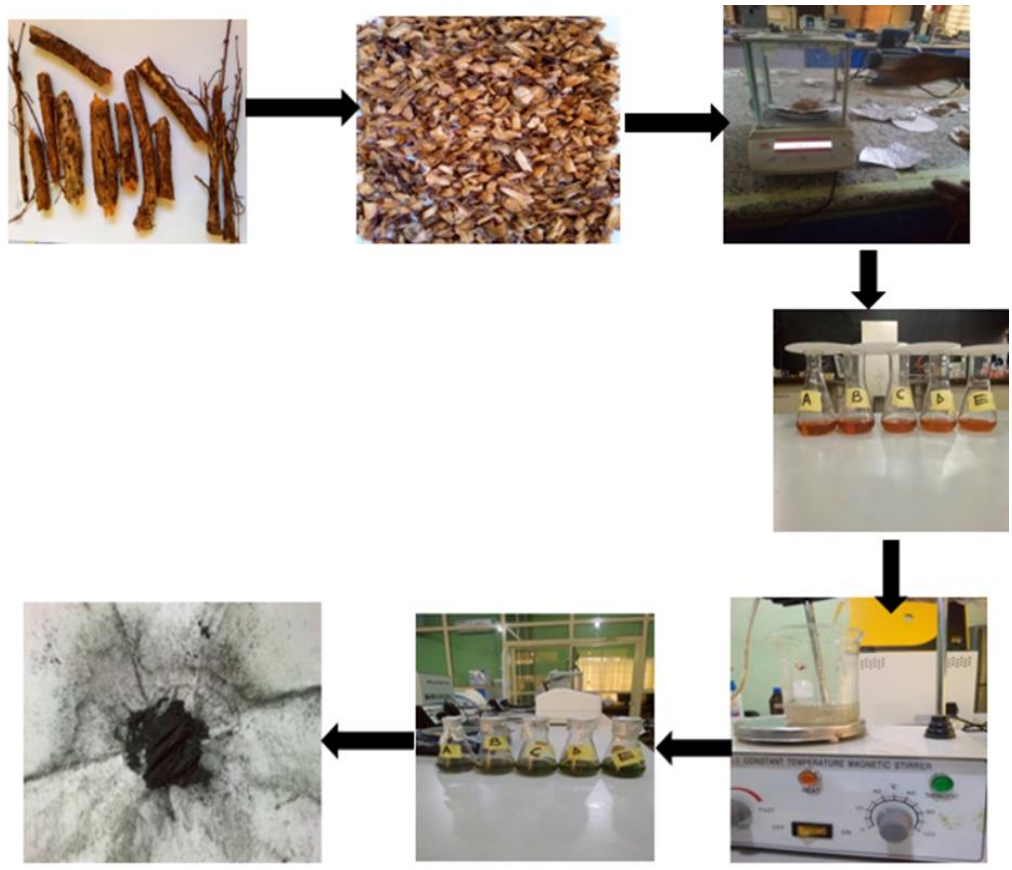

Fig. 3. Schematic diagram of synthesis of AgNPs.

Characterisation of Synthesised AgNPs

An optical spectrophotometer, the UV-Vis, was employed. The transmittance, absorbance and reflectance of the nanoparticles were measured. The optical absorption spectra of biosynthetic AgNPs within the range of 300–1 000 nm were verified and recorded using an ultraviolet spectroscopy (sp-3000 plus optima) in response to the colour shift that transpired in the medium containing the plant extract and the silver nitrate solution. Using a Shimadzu IR Prestige-21 FT-IR spectrophotometer, the attenuated total reflection Fourier transform infrared (ATR/FTIR) spectra of the AgNPs (powder form) were meticulously recorded. Using an X-ray diffractometer (Rigaku Co., Japan), the produced crystallinity of the AgNPs was verified. Using CuKα (λ = 1.5406 Å) radiation with 30 mA of current and 40 kV of voltage at a scan rate of 10°/min over the 2θ angle spanning from 0 °C to 90 °C [35]–[38] the diffractogram was obtained from the dried layer of the sample over a sample holder. Using a scanning electron microscope spectrometer operating at 15 keV, the morphology of AgNPs was examined.

Results and Discussion

X-Ray Diffraction (XRD) Analysis

Using the Panalytical X'pert Pro MRD XRD apparatus with Cu K radiation (λ = 1.5406 Å), the X-ray crystallography method was used to evaluate the crystalline property of green produced NPs throughout a scanning range of 2θ = 0°–70°, with a step size of 0.02°. For samples A to E, the XRD patterns in Fig. 4 show extremely sharp peaks, suggesting that the generated NPs are crystalline in form. According to the investigation, the produced AgNPs have a face-centred cubic (FCC) structure [17].

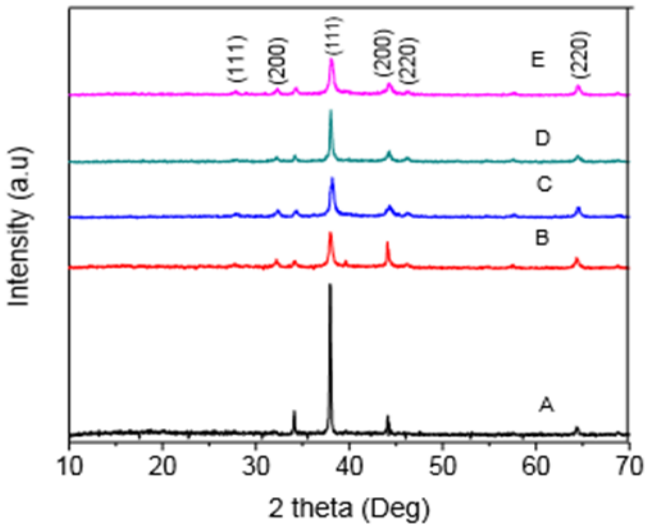

Fig. 4. XRD spectra of the synthesised samples.

The XRD pattern of the synthesised AgNPs for sample A has three peaks positioned at $2\theta = 37.935°$, 44.073° and 64.37° corresponding to (111), (200) and (220) planes, respectively. Thereafter, the peaks of sample B increases with five main peaks positioned at $2\theta = 32.27°$, 37.951°, 44.084°, 46.23° and 64.41° corresponding to (200), (111), (200), (220) and (220) planes, respectively. In sample C, the number of peaks increased with six main peaks at $2\theta = 27.89°$, 32.36°, 38.12°, 44.33°, 46.25° and 64.51° corresponding to (111), (200), (111), (200), (220) and (220) planes, respectively. So also for sample D with six main peaks position at $2\theta = 32.29°$, 37.99°, 44.29°, 46.19°, 57.54° and 64.38° corresponding to (200), (111), (200), (220), (222) and (220) planes, respectively. Finally, sample E exhibits six main peaks at $2\theta = 27.92°$, 32.30°, 38.02°, 44.21°, 46.17° and 64.48° corresponding also to (111), (200), (111), (200), (220) and (220), planes, respectively. The three peaks at 37.99°, 44.29° and 64.38° corresponding to (111), (200) and (220) were reported earlier by Ali *et al*. [1]. The samples have a preferred orientation at $2\theta = 37.94°$ corresponding to (111) plane irrespective of the duration of immersion of *Adansonia digitata* root extracts. The preferred intense peak shows the polycrystalline phase composition of the green synthesised AgNPs, demonstrating the creation of FCC crystalline AgNPs. The number of peaks of the samples increased as the duration of immersion of *Adansonia digitata* root extracts increased. Equation (1) illustrates the application of the well-known Debye–Scherrer equation to determine the crystallite size (D) of AgNPs [39].

$$D = \frac{k\lambda}{\beta \cos\theta} \tag{1}$$

The value of k, an empirical constant dependent on the shape of the crystallite, is 0.89 or 0.9, λ is the X-ray wavelength equivalent to 0.15406 nm, β is the full width at half maximum (FWHM) in radians, and θ is the Bragg angle as presented in Table I.

TABLE I
XRD PROPERTY FOR DIFFERENT SAMPLES

Sample	**2θ**	**β (°)**	***hkl***	**D (nm)**	**d (nm)**	**a (nm)**	**r (nm)**	**V_c**	**V_s**
A	37.94	0.134	111	37.16	0.237	0.4104			
	44.07	0.038	200	143.85	0.205	0.4100			
	64.37	0.180	220	50.48	0.145	0.4101			
			Average	77.16	0.196	0.4088	0.144957	0.068921	0.051058
B	37.95	0.36	111	10.91	0.237	0.4100			
	44.08	0.15	200	26.17	0.205	0.4100			
	64.41	0.30	220	13.09	0.145	0.4100			
			Average	16.72	0.196	0.4100	0.144957	0.068921	0.051058
C	38.12	0.45	111	11.09	0.236	0.4087			
	44.33	0.69	200	7.96	0.204	0.4080			
	64.51	0.44	220	20.76	0.144	0.4072			
			Average	13.27	0.195	0.4080	0.14425	0.067917	0.050314
D	37.99	0.19	111	26.23	0.237	0.4105			
	44.29	0.43	200	12.76	0.204	0.4080			
	64.38	0.55	220	16.53	0.145	0.4101			
			Average	18.51	0.195	0.4095	0.144603	0.068418	0.050684

Sample	2θ	β (°)	*hkl*	D (nm)	d (nm)	a (nm)	r (nm)	V_c	V_s
E	38.02	0.42	111	11.87	0.236	0.4087			
	44.21	0.49	200	11.18	0.205	0.4100			
	64.48	0.26	220	35.09	0.144	0.4072			
			Average	19.38	0.195	0.4086	0.144603	0.068418	0.050684

From Fig. 4, the XRD peaks positions and width are the same for all samples (A to E), but the intensity of the peaks is not the same. This could indicate a difference in the amount of crystallinity of the samples analysed. The number of atoms in the crystal that may scatter X-rays determines the strength of the XRD peak [40].

Sample A, therefore, has a higher preferred peak intensity which attributes to a higher number of atoms in the crystal, indicating a higher degree of crystallinity or a crystal size. Sample C has the lowest preferred peak intensity, which suggests that sample C has a lower degree of crystallinity or crystal size [41].

The peak intensities of the samples decreased as the duration of immersion of *Adansonia digitata* root powder increased. This suggests that the higher the immersion time of *Adansonia digitata* root powder the lower the crystal sized.

The lattice parameter, *a*, is calculated for each peak position using equation (2).

$$a = d\sqrt{h^2 + k^2 + l^2} \tag{2}$$

Samples A, B, C, D and E have average lattice parameters of 0.4088, 0.4100, 0.4080, 0.4095 and 0.4086 nm, respectively. These lattice values are quite similar to the AgNPs lattice parameter of 0.4086 nm, which is listed in JCPDS file number 04-0783.

The produced AgNPs have an average unit cell edge of a = 0.408 nm and an FCC crystal structure. The produced radius, *r*, of the synthesised AgNPs is calculated using equation (3).

$$r = \frac{a\sqrt{2}}{4} \tag{3}$$

The radii, *r*, for samples A, B, C, D and E are found to be 0.144957 nm, 0.144957 nm, 0.14425 nm, 0.144603 nm and 0.144603 nm for the synthesised AgNPs. The calculated radii for all samples are in agreement.

The volume of atomic spheres (V_s) divided by the volume of a unit cell (V_c) is known as the atomic packing factor (APF). The APF can be obtained using equation (4).

$$APF = \frac{4\times\frac{4}{3}\pi R^3}{a^3} \tag{4}$$

where $R \approx r$. The AgNPs' FCC crystal structure and closely packed atoms inside the lattice structure are confirmed by the average APF of 0.74 for the entire sample.

The rate of chemical reaction is calculated using the surface area (S) to volume (V) ratio and can be determined using equation (5).

$$S/V = \frac{4\pi R^2}{\frac{4}{3}\pi R^3} \tag{5}$$

The ratio of surface area to volume is 20×10^9, which is quite high. It implies that the synthesised NPs have a sufficient large surface to react because of an extremely small radius.

The lattice strain was estimated from the Williamson-Hall plot of $\beta \cos \theta$ against 4 sin θ using equation (6).

$$\beta \cos\theta = 4\epsilon \sin\theta + \frac{0.89}{D} \tag{6}$$

where ϵ is the lattice strain. Plotting (Fig. 5) provides ϵ as the slope and D as the value inferred from the plot's intercept. The D of the synthesised AgNPs was determined and presented in Table II.

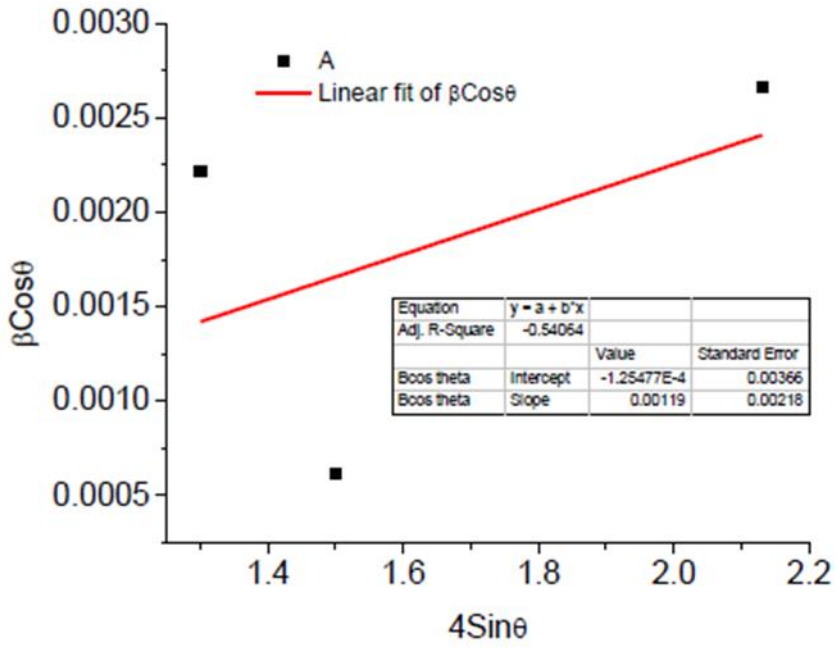

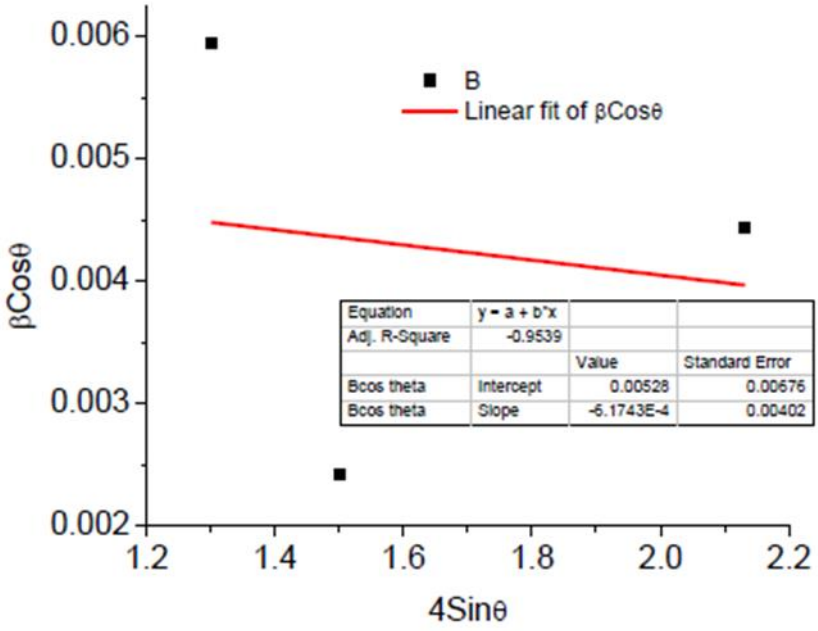
B
Linear fit of βCosθ
βCosθ
4Sinθ
0.006
0.005
0.004
0.003
0.002
1.2
1.4
1.6
1.8
2.0
2.2
Equation y = a + b*x
Adj. R-Square -0.9539
Value Standard Error
Bcos theta Intercept 0.00528 0.00676
Bcos theta Slope -6.1743E-4 0.00402

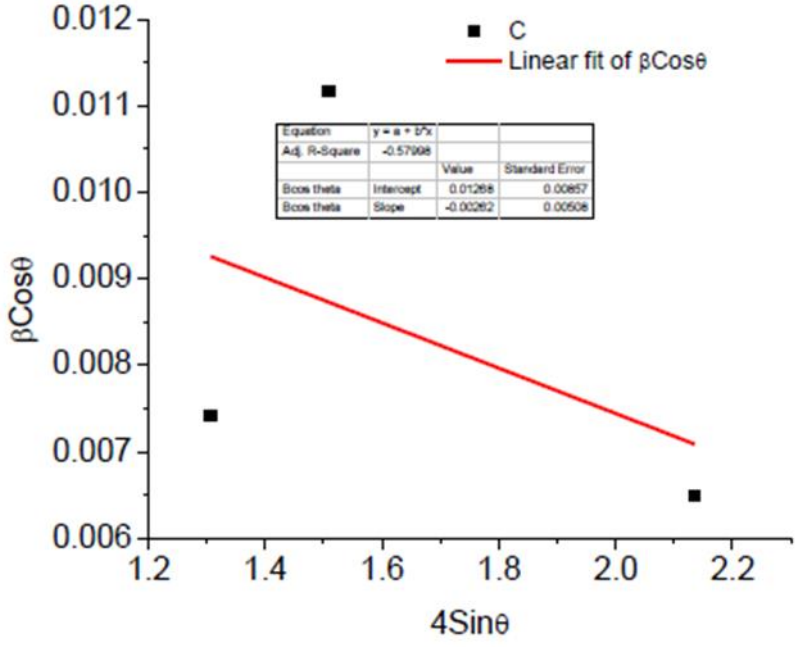
C
Linear fit of βCosθ
βCosθ
4Sinθ
0.012
0.011
0.010
0.009
0.008
0.007
0.006
1.2
1.4
1.6
1.8
2.0
2.2
Equation y = a + b*x
Adj. R-Square -0.57908
Value Standard Error
Bcos theta Intercept 0.01268 0.00857
Bcos theta Slope -0.00282 0.00508

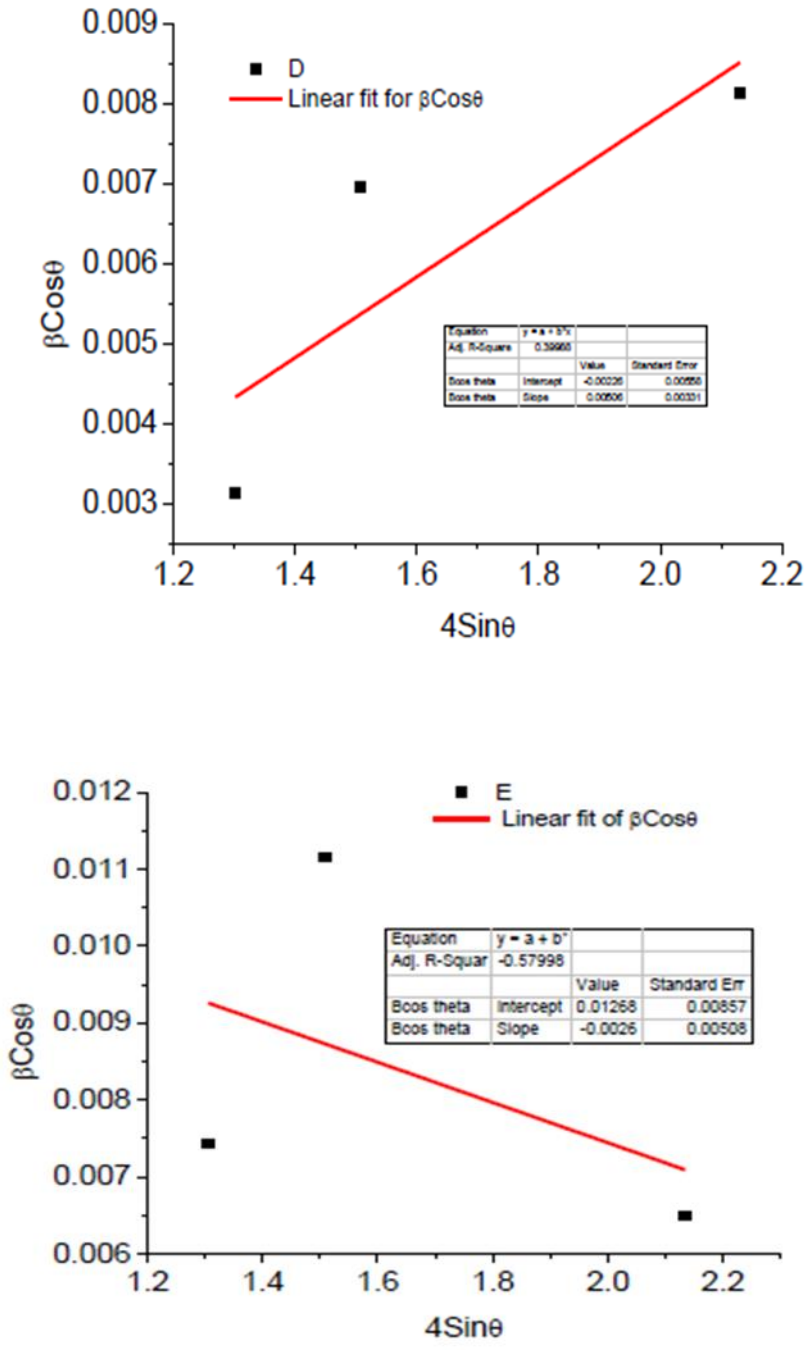

Fig. 5. Plot of the produced AgNPs using the Williamson-Hall method.

The intrinsic stress, σ_s, present in the NPs, is caused by a departure from the bulk lattice constant of AgNPs as observed. It is calculated using equation (7).

$$\sigma_s = \frac{Y(a-a_0)}{2a_0\gamma} \quad (7)$$

where Y is the Young modulus of the AgNPs (83 GPa), a is lattice constant of the NPs, a_0 is the bulk lattice constant (0.4086 nm) and γ is the is the Poisson ratio (0.37). The intrinsic stresses of the samples are presented in Table II.

TABLE II
WILLIAMSON-HALL PLOTTING DATA

Sample	**Lattice strain ϵ $\times 10^{-4}$**	**Intrinsic stress (GPa)**	**Dislocation density δ (m^2)**	***S/V*** **$\times 10^{-4}$**
A	1.19	0.0549	2.63×10^{-4}	2.070
B	6.17	0.3843	3.36×10^{-4}	2.070
C	2.68	−0.1647	1.84×10^{-3}	2.080
D	5.06	0.2471	2.94×10^{-3}	2.074
E	2.62	0.0	1.15×10^{-3}	2.074

The dislocation density or the quantity of dislocations per unit volume (δ) of the crystal was determined using equation (8). Smaller δ values indicate higher degrees of crystallinity in NPs.

$$\delta = \frac{15\beta\cos\theta}{4aD} \quad (8)$$

One of the primary determinants of the degree of distortion in a regular atomic array with flawless crystal structure is the existence of dislocation in NPs. Table II presents the mean values of the prepared samples.

The specific surface area, *S*, of NPs is particularly important in relation to their particle size. The particular surface area and particle size are inversely related. The two factors are crucial components of NPs because of the link that exists between them. The corresponding values of *S* for each sample are found using the Brunauer-Emmett-Teller equation (9).

$$S = \frac{6\times10^3}{D_p\times\rho} \quad (9)$$

D_p is the particle size of the NPs, ρ is the density of AgNPs (10.5 gcm^3).

All the samples indicate the presence of boleite and chloargyrite at various proportions as shown in Fig. 6. The charts were obtained from the XRD analysis. The percentage of AgNPs synthesised increased from A to B at 70% and 73%, respectively. A further

increase in immersion time of the extracts indicates a decrease in the percentage of synthesised AgNPs from C to E. The chart suggests that the optimised immersion time of the extracts is 60 min (sample B).

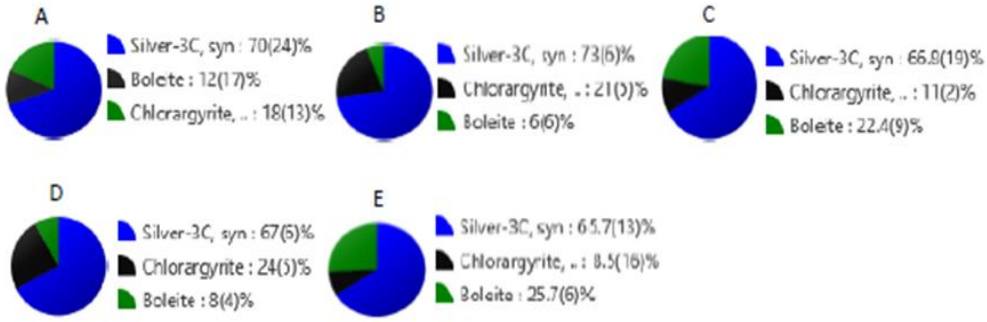

Fig. 6. Percentage distribution of silver nanoparticles of different samples of immersion time.

Morphological Study of Synthesised AgNPs

A field emission scanning electron microscopy (FESEM) was used to study the synthesised AgNPs of different sizes and shapes to gain additional insight into nanostructured materials. Fig. 7(a) to (e) shows examples of the AgNPS made with the *Adansonia digitata* extract. AgNPs are typically found in a variety of forms, including dendrites, nanorods, nanoplates, nanocubes, nanospheres and nanowires. They can even resemble flowers. According to Shenashen *et al*. [42], AgNPs made from plant extracts have a mostly spherical form. There are diverse sizes and shapes of the AgNPs with peculiar characteristics attributed to individual samples.

AgNPs are stable and sensitive because of their large specific surface area, high surface reaction and well-organised transmission channel that allows the analyte molecules to reach the active sites. The particle sizes obtained from the SEM analysis are 69.88, 18.69, 15.45, 19.64 and 20.08 nm for samples A, B, C, D and E, respectively. The particle sizes of the samples decreased from samples A to C in SEM samples. Thereafter, the particle size increased from samples D to E. The particle size change does not have a regular pattern as in the case of XRD analysis. The result of the SEM analysis is in agreement with that of XRD analyses.

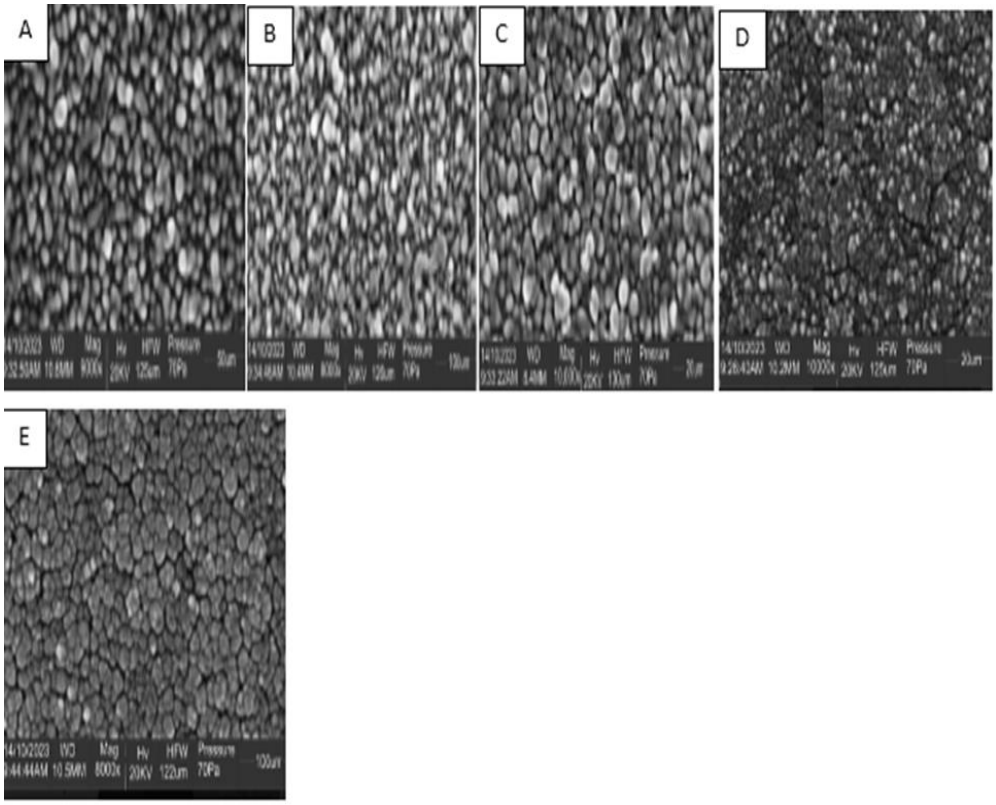

Fig. 7. SEM images of synthesised AgNPs.

UV-Visible Analysis of AgNPs

UV-Vis spectroscopy, which appears to be a particularly helpful approach in the investigation of nanoparticles, was used to characterise the AgNPs. Fig. 8 shows the UV-Vis spectroscopy of AgNPs where absorbance is plotted against wavelength. There is a presence of one absorption peak for each sample located at 370.53 nm and 377.32 nm for samples A and E respectively, 372.20 nm for sample B, 373.06 nm for sample C and 369.68 nm for sample D. The absorption peaks are at near ultraviolet regions of electromagnetic spectrum. The absorption peak reported here correspond to an earlier report by Periasamy *et al*. [43] on the flower of *Hibiscus rosasinensis* at a maximum absorption peak of 357 nm.

Nevertheless, the maximum absorption peaks in the study are lower than those of the silver nanoparticle obtained from *Hibiscus rosasinensis* leaf and bark extracts as reported by Periasamy *et al*. [43]. This is as a result of certain silver ions found in the sample particle made of the *Adansonia digitata* stem extract. The absorption spectra of the samples do not follow a regular pattern. The intensity of absorption peak of the samples decreased as the duration of immersion of the *Adansonia digitata* root powder

increased to 60 min for sample B. After that, as the immersion time of the *Adansonia digitata* root extract increased to 90 min, the strength of the absorption peak of sample C increased as well. For sample D, the strength of the absorption peak decreased. The intensity of the absorption peak of sample E increased at a duration of 150 min. The absorption of the sample increased as the duration of immersion *Adansonia digitata* root powder increased. Meanwhile, the absorption peaks for all samples shows that absorption of sample E is the highest.

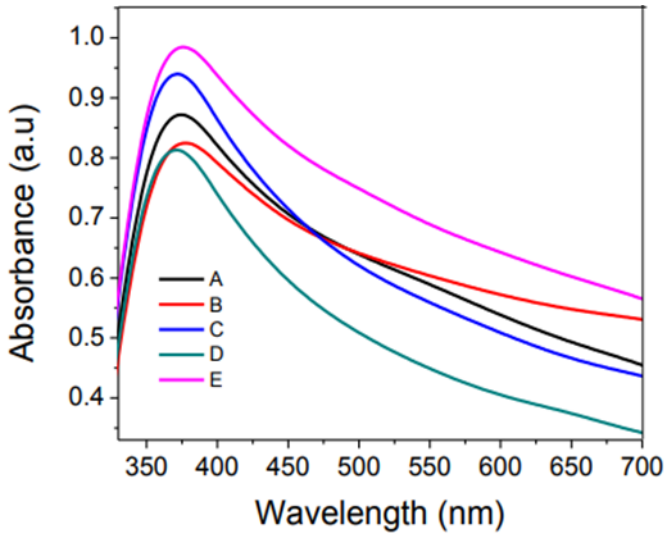

Fig. 8. UV-Vis spectra of synthesised AgNPs at different durations of immersion.

The difference in the number of peaks presented in Fig. 8 reflects the immersion time difference of the extracts. The absorption peak range in the region (200–400 mm) was very clear in all samples (A, B, C, D and E) indicating that there were unsaturated functional groups and heterozygous atoms such as S, N and O [44].

The colour shift seen in Fig. 8 indicates the reduction of silver ions (Ag^{+}) into AgNPs (Ag^{0}) upon exposure to plant extracts from the *Adansonia digitata* species. The phenomenon known as surface plasmon resonance (SPR) is what causes the colour shift. The SPR absorption band is produced by the free electrons in the metal nanoparticles, which are coupled to vibrate in resonance with light waves [45]. Visual observation of the reaction solution's colour changing from colourless to dark brown indicates the creation of AgNPs during the reduction phase.

The varying sizes of the manufactured particles may be the cause of the samples' varying light absorption. In addition, lower and higher and absorptions show smaller and larger nanoparticle sizes, respectively [46].

The optical band gap energy of AgNPs was estimated from the Tauc's relation (Fig. 9). Fig. 9 shows the plot of $(\alpha h\nu)^2$ against photon energy ($h\nu$) for allowed direct transition [47]–[49] of AgNPs at different immersion times of the *Adansonia digitata* root extract. The energy and gap deduced from Tauc's plot is presented in Table III. Table III presents that the different optical energy band gaps are 2.37 eV, 2.42 eV, 2.59 eV, 2.52 eV and 2.34 eV for samples A, B, C, D and E, respectively. It indicates an increase in the energy band gap from samples A to C and a decrease in the energy band gap from samples D to E.

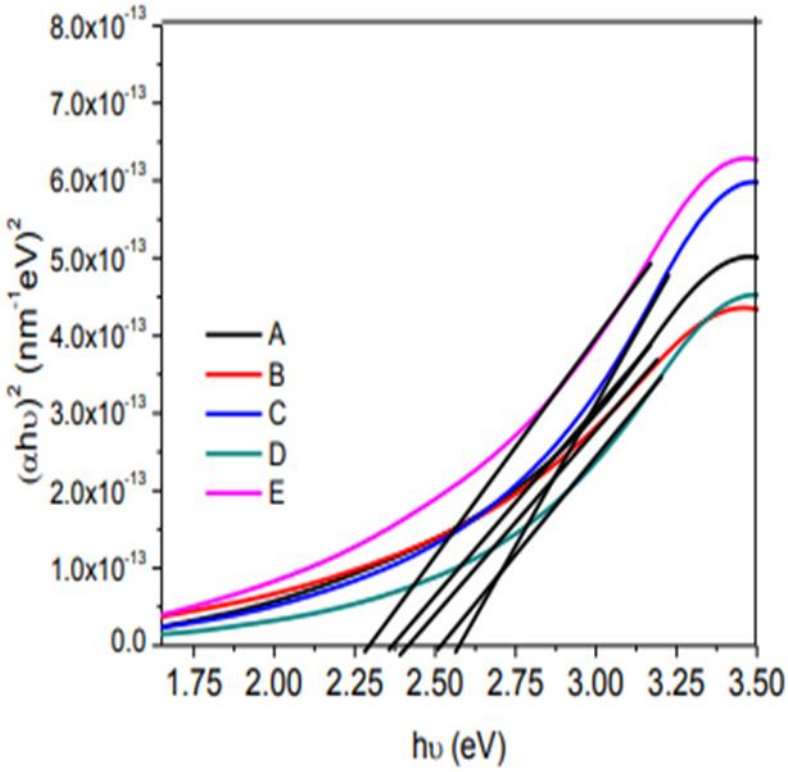

Fig. 9. Tauc's plot for energy band gaps of synthesised AgNPs.

TABLE III
OPTICAL PROPERTY OF SYNTHESISED SAMPLES

Sample	Absorption range (nm)	Absorption peak (nm)	Tauc's plot energy band gap (eV)
A	338.72–473.46	370.53	2.37
B	339.82–473.46	372.20	2.42
C	335.33–473.46	373.06	2.59
D	339.82–457.62	369.68	2.52
E	335.33–484.81	377.32	2.34

Fourier-Transform Infrared Spectroscopy

For the capping of bio-reduced AgNPs produced by *Adansonia digitata* root extracts and the reduction of Ag^{+} ions, the chemical compositions of the AgNP surfaces were investigated using the Fourier-transform infrared (FTIR) spectroscopy; likely biomolecules that were involved were found. Transmittance (%) is plotted against wave number (cm^{-1}). The FTIR spectra of the biosynthesised AgNPs for each sample show different peaks (Fig. 10). Samples A and B have the same number of peaks, which shows that the numbers of peaks for samples A and B remain the same as the duration of immersion of *Adansonia digitata* root extracts increased to 60 min for sample B where the number of peaks decreased. Similarly, samples C and D have the same number of peaks as the duration of immersion of *Adansonia digitata* root extracts increased to 120 min for sample D.

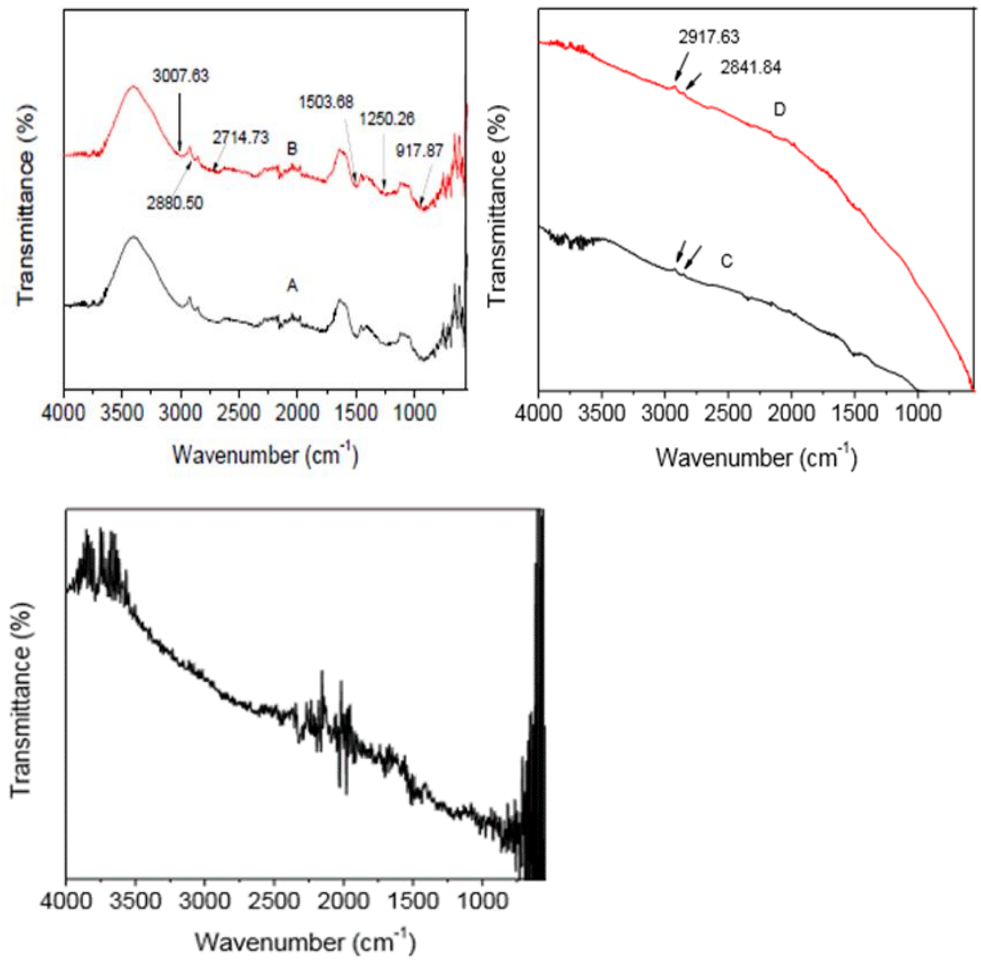

Fig. 10. FTIR spectrum of the synthesised AgNPs samples.

The number of peaks for sample E decreased after a duration of 120 min. The N-H stretching vibration of protein amides and the O-H group in alcohols and phenols are revealed by the peak in the FTIR spectra of samples A and B at 3 007.63 cm^{-1} [50]. The peaks in the FTIR spectra of samples A and B at 2 880.50 cm^{-1} and 2 714.73 cm^{-1} were caused by the alkynes in the -CC- band. Samples C and D show shifts in the peak positions. The shifted peaks correspond to the CC- band of alkynes at 2 917.63 cm^{-1} and 2 841.84 cm^{-1} in the FTIR spectrum. The -C = C- band of alkenes caused a peak at 1 503.68 cm^{-1}. Amide I and Amide II bands, resulting from carbonyl (C = O) and amine (NH) stretching vibrations in the protein amide linkages, were also seen in the FTIR spectrum at 1 250.26 cm^{-1} and 917.87 cm^{-1}, respectively. Alcohols and carboxylic acids underwent C-O stretching. The biosynthesised AgNPs in samples A, B, C and D all have the same absorption band locations in the FTIR spectra, but sample D exhibits no peak and is completely different from the other samples. The FTIR spectra of the synthesised AgNPs show that sample B (synthesised at 60 min) is the optimised sample and the result agrees with the outcome of XRD and UV-Vis analyses.

Conclusion

In this article, we report on the production of AgNPs using $AgNO_3$ as a metal precursor and an extract of *Adansonia digitata* stem extracts as a reducing agent. First, a complete conversion reaction was verified by the $AgNO_3$ solution and *Adansonia digitata* stem extracts mixture's colour changing from yellow to brown over the course of the reaction. The samples' typical average size range of 13.27 to 77.16 nm was determined using the Debye-Scherrer equation, showing the presence of a nanocrystal. The XRD analysis verified the nanoparticle's FCC crystalline structure, with the (111) plane serving as the prominent peak. The values of lattice strain (ε), intrinsic stress (δ_s), dislocation density (δ), unit cell volume (V_c), and atomic packing fraction (APF) were $(1.19 – 6.17) \times 10^{-4}$, 0.1647–0.2471 GPa, $2.63 \times 1\ 010^{-4} \times 10^{-2} nm^2$, 0.068 nm^3 and 0.74, respectively. The maximum absorption peaks of all the samples were found at the UV region of the electromagnetic spectrum. The energy band gaps of all the synthesised samples were within 2.34 eV to 2.59 eV with sample B having an energy band gap value of 2.42 eV. The FTIR result showed the possible formation of AgNPs. Samples A and B had the same number of peaks, which showed that the numbers of peaks for samples A and B remain the same as the duration of immersion of *Adansonia digitata* root extracts increased to 60 min for sample B where the number of peaks decreased. Similarly, samples C and D had the same number of peaks as the duration of immersion of *Adansonia digitata* root extracts increased to 120 min for sample D. The number of peaks for sample E therefore decreased after a duration of 120 min.

The results showed that there was a level of reduction, and that sample B (60 min) was the optimised immersion time of *Adansonia digitata* root extracts.

Acknowledgements

We thank the Central Laboratory at Modibbo Adama University in Yola for making its facilities available during this study.

References

[1] Md. H. Ali, Md. A. K. Azad, K. A. Khan, Md. O. Rahman, U. Chakma and A. Kumer, "Analysis of crystallographic structures and properties of silver nanoparticles synthesized using PKL extract and nanoscale characterization techniques," *ACS Omega*, vol. 8, no. 31, pp. 28133−28142, July 2023, doi: 10.1021/acsomega.3c01261.

[2] A. Bazrgaran, S. Mahmoodabadi, A. Ghasempour, E. Shafaie, A. Sahebkar and S. Eghbali, "Facile bio-genic synthesis of *Astragalus sarcocolla* (Anzaroot) gum extract mediated silver nanoparticles: Characterizations, antimicrobial and antioxidant activities," *Plant Nano Biol.*, vol. 6, p. 100052, November 2023, doi: 10.1016/j.plana.2023.100052.

[3] G. M. Nair, T. Sajini and B. Mathew, "Advanced green approaches for metal and metal oxide nanoparticles synthesis and their environmental applications," *Talanta Open*, vol. 5, p. 100080, August 2022, doi: 10.1016/j.talo.2021.100080.

[4] M. Ibrahim, "Current perspectives of nanoparticles in medical and dental biomaterials" *J. Biomed. Res*., vol. 26, no. 3, pp. 143−151, April 2012, doi: 10.7555/JBR.26.20120027.

[5] N. M Basfer and N. Al-Harbi, "Structural, optical and photocatalytic activity of Ce^{3+} doped Co–Mg nanoparticles for wastewater treatment applications," *J. King Saud Univ.Sci.*, vol. 35, no. 1, p. 102436, January 2023, doi: 10.1016/j.jksus.2022.102436.

[6] S. Panimalar *et al*., "Effect of Ag doped MnO_2 nanostructures suitable for wastewater treatment and other environmental pollutant applications," *Env. Res.*, vol. 205, p. 112560, April 2022. doi: 10.1016/j.envres.2021.112560.

[7] L. G. Bousiakou, P. J. Dobson, T. Jurkin, I. Marić, O. Aldossary and M. Ivanda, "Optical, structural and semiconducting properties of Mn doped TiO_2 nanoparticles for cosmetic applications," *J. King Saud Univ. Sci.*, vol. 34, no. 3, p. 101818, April 2022, doi: 10.1016/j.jksus.2021.101818.

[8] S. R. Al-Mhyawi, "Green synthesis of silver nanoparticles and their inhibitory efficacy on corrosion of carbon steel in hydrochloric acid solution," *Int. J. Electrochem. Sci.*, vol. 18, no. 9, p. 100210, September 2023, doi: 10.1016/j.ijoes.2023.100210.

[9] J. Y. Song and B. S. Kim, "Rapid biological synthesis of silver nanoparticles using plant leaf extracts," *Bioprocess Biosyst. Eng*., vol. 32, pp. 79–84, April 2009, doi: 10.1007/s00449-008-0224-6.

[10] F. Okafor, A. Janen, T. Kukhtareva, V. Edwards and M. Curley, "Green synthesis of silver nanoparticles, their characterization, application and antibacterial activity," *Int. J. Environ. Res. Public Health*, vol. 10, no. 10, pp. 5221–5238, October 2003, doi: 10.3390/ijerph10105221.

[11] N. Rani, P. Singh, S. Kumar, P. Kumar, V. Bhankar and K. Kumar, "Plant-mediated synthesis of nanoparticles and their applications: A review," *Mater. Res. Bull.*, vol. 163, p. 112233, July 2023, doi: 10.1016/j.materresbull.2023.112233.

[12] S. Ying, Z. Guan, P. C. Ofoegbu, P. Clubb, C. Rico, F. He and J. Hong, "Green synthesis of nanoparticles: Current developments and limitations," *Environ. Technol. Innov.*, vol. 26, p. 102336, May 2022, doi: 10.1016/j.eti.2022.102336.

[13] D. Garg *et al.*, "Synthesis of silver nanoparticles utilizing various biological systems: Mechanisms and applications – A review," *Prog. Biomater*, vol. 9, pp. 81−95, July 2020, doi: 10.1007/s40204-020-00135-2.

[14] I. Uluisik, H. C. Karakaya and A. Koc, "The importance of boron in biological systems," *J. Trace Elem. Med. Biol.*, vol. 45, pp. 156−162, January 2018, doi: 10.1016/j.jtemb.2017.10.008.

[15] K. B. Narayanan and N. Sakthivel, "Green synthesis of biogenic metal nanoparticles by terrestrial and aquatic phototrophic and heterotrophic eukaryotes and biocompatible agents," *Adv. Colloid Interface Sci.*, vol. 169, no. 2, pp. 59−79, December 2011, doi: 10.1016/j.cis.2011.08.004.

[16] I. Li, H. Zeng, Z. Zeng, Y. Zeng and T. Xie, "Promising grapheme-based nanomaterials and their biomedical applications and potential risks: A comprehensive review," *ACS Biomater. Sci. Eng.*, vol. 7, no. 12, pp. 5363−5396, November 2021, doi: 10.1021/acsbiomaterials.1c00875.

[17] I. Khan, K. Saeed and I. Khan, "Nanoparticles: Properties, applications and toxicities," *Arabian J. Chem.*, vol. 12, no. 7, pp. 908−931, November 2019, doi: 10.1016/j.arabjc.2017.05.011.

[18] H. Jan *et al.*, "A detailed review on biosynthesis of platinum nanoparticles (PtNPs), their potential antimicrobial and biomedical applications," *J. Saudi Chem. Soc.*, vol. 25, no. 8, p. 101297, August 2021, doi: 10.1016/j.jscs.2021.101297.

[19] R. Javed, M. Zia, S. Naz, O. Aisida, N. ul Ain and O. Ao, "Role of capping agents in the application of nanoparticles in biomedicine and environmental remediation: recent trends and future prospects," *J. Nanobiotechnology*, vol. 18, p. 172, November 2020, doi: 10.1186/s12951-020-00704-4.

[20] L. Cieśla, I. Kowalska, W. Oleszek and A. Stochmal, "Free radical scavenging activities of polyphenolic compounds isolated from *Medicago sativa* and *Medicago truncatula* assessed by means of thin-layer chromatography DPPH rapid test," *Phytochem. Anal.*, vol. 24, no. 1, pp. 47–52, January 2013, doi: 10.1002/pca.2379.

[21] O. V. Kharissova, H. V. Dias, B. I. Kharisov, B. O. Perez and V. M. Perez, "The greener synthesis of nanoparticles," *Trends Biotechnol*., vol. 31, no. 4, pp. 240–248, April 2013, doi: 10.1016/j.tibtech.2013.01.003.

[22] M. Tomita and M. Murakami, "High-temperature superconductor bulk magnets that can trap magnetic fields of over 17 tesla at 29 K," *Nature*, vol. 421, pp. 517−520, January 2003, doi: 10.1038/nature01350.

[23] U. K. Sur, "Biosynthesis of metal nanoparticles and graphene," in *Advanced Surface Engineering Materials*, A. Tiwari, R. Wang and B. Wei, Eds, John Wiley & Sons, 2016, ch. 6, pp. 241−295, doi: 10.1002/9781119314196.ch6.

[24] X. Han and L. L. Parker, "Lemongrass (*Cymbopogon flexuosus*) essential oil demonstrated anti-inflammatory effect in pre-inflamed human dermal fibroblasts," *Biochim. Open*, vol. 4, pp. 107−111, June 2017, doi: 10.1016/j.biopen.2017.03.004.

[25] S. Pouyan, K. Kafshdouzan and A. Jebelli, "Synergistic effect of Cinnamomum camphora and Origanum vulgare essential oils against bla CTX-M producing Escherichia coli isolated from poultry colibacillosis," *J. Med. Bacteriol*., vol. 10, no. 1–2, pp. 20−29, 2021, https://jmb.tums.ac.ir/index.php/jmb/article/view/444.

[26] J. F. Islas, E. Acosta, G. Zuca, J. L. Delgado-Gallegos, M. G. Moreno-Treviño, B. Escalante and J. E. Moreno-Cuevas, "An overview of neem (*Azadirachta indica*) and its potential impact on health," *J. Funct. Foods*, vol. 74, p. 04171, November 2020, doi: 10.1016/j.jff.2020.104171.

[27] A. N. Ossai, S. C. Ezike and A. B. Dikko, "Bio-synthesis of zinc oxide nanoparticles from bitter leaf (*Vernonia amygdalina*) extract for dye-sensitized solar cell fabrication," *J. Mater. Environ. Sci.*, vol. 1, pp. 444–451, 2020.

[28] A. Surjushe, R. Vasani and D. G. Saple, "Aloe vera: A short review," *Indian J. Dermatol*. vol. 53, no. 4, pp. 163−166, October 2008, doi: 10.4103/0019-5154.44785.

[29] A. H. A. Al-Jobouri, "Studying some the functional properties of tamarind tamarindus indica L. Mucilage," *Al-Qadisiyah J. Agric. Sci*., vol. 10, no. 2, pp. 304−307, December 2020, doi: 10.33794/qjas.2020.167474.

[30] S. Phochantachinda, D. Chatchaisak, P. Temviriyanukul, A. Chansawang, P. Pitchakarn and B. Chantong, "Ethanolic fruit extract of *Emblica officinalis* suppresses neuroinflammation in microglia and promotes neurite outgrowth in neuro2a cells," *Evidence-Based Complementary Altern. Med*. pp. 1−16, September 2021, doi: 10.1155/2021/6405987.

[31] A. D. Ahmed, B. D. V. Mathew, S. C. Ezike and P. Timtere, "Effects of treatment duration on mechanical, chemical, structural and thermal properties of baobab-pod fibres," *J. Nat. Fibres*, vol. 19, no. 16, pp. 15116–15127, May 2022, doi: 10.1080/15440478.2022.2070326.

[32] D. E. Isaac, M. I. Monday and B. A. Abel, "Evaluation of *Adansonia digitata* (baobab) leaf and root extracts as inhibitor on dual phase steel (DPS) in 0.3M H2SO4," *American Journal of Computing and Engineering*, vol. 5, no. 2, pp. 15–23, 2022, doi: 10.47672/ajce.1261.

[33] U. I. Ndeze, J. Aidan, S. C. Ezike and J. F. Wansah, "Comparative performances of nature-based dyes extracted from baobab and shea leaves photo-sensitizers for dye-sensitized solar cells (DSSCs)," *Curr. Res. Green Sustain. Chem.*, vol. 4, p. 100105, 2021, doi: 10.1016/j.crgsc.2021.100105.

[34] M. Ali and B. H. Abbasi, "Light-induced fluctuations in biomass accumulation, secondary metabolites production and antioxidant activity in cell suspension cultures of *Artemisia absinthium* L.," *J. Photochem. Photobiol. B*, vol. 140, pp. 223–227, November 2014, doi: 10.1016/j.jphotobiol.2014.08.008.

[35] H. P. Wante, J. Aidan and S. C. Ezike, "Efficient dye-sensitized solar cells (DSSCs) through atmospheric pressure plasma treatment of photoanode surface", *Curr. Res. Green Sust. Chem.*, vol. 4, p. 100218, 2021, doi: 10.1016/j.crgsc.2021.100218.

[36] B. Alkali, J. B. Yerima, A. D. Ahmed and S. C. Ezike, "Suppressed charge recombination aided co-sensitization in dye-sensitized solar cells-based natural plant extracts". *Optik*, vol. 270, p. 170072, November 2022, doi: 10.1016/j.ijleo.2022.170072.

[37] S. C. Ezike, A. B. Alabi, A. N. Ossai and A. O. Aina, "Stability-improved perovskite solar cells through 4-tertbutylpyridine surface-passivated perovskite layer fabricated in ambient air", *Opt. Mater.*, vol. 112, p. 110753, February 2021, doi: 10.1016/j.optmat.2020.110753.

[38] A. D. Ahmed, S. C. Ezike, E. Ike, K. H. Idu, R. M. Obodo and M. A. Salawu, "Spray pyrolyzed surface-modified ZnO thin films via cobalt doping: Optical, structural and morphological properties," *Opt. Mater.*, vol. 149, p. 115053, March 2024, doi: 10.1016/j.optmat.2024.115053.

[39] A. N. Ossai, A. B. Alabi, S. C. Ezike and A. O. Aina, "Zinc oxide-based dye-sensitized solar cells using natural and synthetic sensitizers," *Curr. Res. Green Sust. Chem.*, vol. 3, p. 100043, June 2020, doi: 10.1016/j.crgsc.2020.100043.

[40] A. Ali, Y. W. Chiang and R. M. Santos, "X-ray diffraction techniques for mineral characterization: A review for engineers of the fundamentals, applications, and research directions," *Minerals*, vol. 12, no. 2, p. 205, February 2022, doi: 10.3390/min12020205.

[41] M. A. Adekoya, S. Liu, S. S. Oluyamo, O. T. Oyeleye and R. T. Ogundare, "Influence of size classifications on the crystallinity index of *Albizia gummifera* cellulose," *Heliyon*, vol. 8, no. 12, p. e12019, December 2022, doi: 10.1016/j.heliyon.2022.e12019.

[42] M. A. Shenashen, S. A. El-Safty and E. A. Elshehy, “Synthesis, morphological control, and properties of silver nanoparticles in potential applications,” *Part. Syst. Charact.*,” vol. 31, no. 3, pp. 293–316, March 2014, doi: 10.1002/ppsc.201300181.

[43] S. Periasamy *et al.*, “Comparative analysis of synthesis and characterization of silver nanoparticles extracted using leaf, flower, and bark of *Hibiscus rosasinensis* and examine its antimicrobicidal activity,” *J. Nanomater.*, vol. 2022, May 2022, doi: 10.1155/2022/8123854.

[44] V. O. Njoku, K. Y. Foo and B. H. Hameed, “Microwave-assisted preparation of pumpkin seed hull activated carbon and its application for the adsorptive removal of 2,4-dichlorophenoxyacetic acid,” *Chem. Eng. J.*, vol. 215–216, pp. 383–388, January 2013, doi: 10.1016/j.cej.2012.10.068.

[45] K. Renugadevi and V. Aswini, “Microwave irradiation assisted synthesis of silver nanoparticle using leaf extract of *Baliospermum montanum* and evaluation of its antimicrobial, anticancer potential activity,” *Asian J. Pharm. Clin. Res.*, vol. 5, pp. 283–287, November 2012.

[46] H. Lin, C. Huang, W. Li, C. Ni, S. Shah and Y. Tseng, “Size dependency of nanocrystalline TiO2 on its optical property and photocatalytic reactivity exemplified by 2-chlorophenol,” *Appl. Catal. B*, vol. 68, no. 1–2, pp. 1−11, October 2006, doi: 10.1016/j.apcatb.2006.07.018.

[47] S. C. Ezike and D. N. Okoli, “Deposition temperature effects on $cualse_2$ compound thin films prepared by chemical bath deposition technique,” *IOSR J. Appl. Phys.*, vol. 1, no. 3, pp. 23–26, July 2012, doi: 10.9790/4861-0132326.

[48] K. A. Uyanga, S. C. Ezike, A. T. Onyedika, A. B. Kareem and T. M. Chiroma, “Effect of acetic acid concentration on optical properties of lead acetate based methylammonium lead iodide perovskite thin film,” *Opt. Mater.*, vol. 109, p. 110456, November 2020, doi: 10.1016/j.optmat.2020.110456.

[49] S. C. Ezike, A. B. Alabi, A. N. Ossai and A. O. Aina, “Effect of tertiary butylpyridine in stability of methylammonium lead iodide perovskite thin films,” *Bull. Mater. Sci.*, vol. 43, p. 40, January 2020, doi: 10.1007/s12034-019-2002-2.

[50] J. O. Ogunkanmi, D. M. Kulla, N. O. Omisanya, M. Sumaila, D. O. Obada and D. Dodoo-Arhin. “Extraction of bio-oil during pyrolysis of locally sourced palm kernel shells: Effect of process parameters,” *Case Studies in Thermal Engineering*, vol. 12, pp. 711–716, September 2018, doi: 10.1016/j.csite.2018.09.003.